

## Electronic Supplementary Information (ESI) for Energy & Environmental Science

### Electronic Structure Engineering to Boost Oxygen Reduction Activity by Controlling the Coordination of Central Metal

Yunhu Han,<sup>‡a</sup> Yanggang Wang,<sup>‡a</sup> Ruirui Xu,<sup>b</sup> Wenxing Chen,<sup>a</sup> Lirong Zheng,<sup>c</sup> Aijuan Han,<sup>a</sup> Youqi Zhu,<sup>a</sup> Jian Zhang,<sup>a</sup> Huabin Zhang,<sup>d</sup> Jun Luo,<sup>e</sup> Chen Chen,<sup>a</sup> Qing Peng,<sup>a</sup> Dingsheng Wang\*<sup>a</sup> and Yadong Li\*<sup>a</sup>

<sup>a</sup>Department of Chemistry Tsinghua University Beijing 100084, China

<sup>b</sup>School of Chemistry & Chemical Engineering, Shaanxi Normal University Xi'an 710000, China.

<sup>c</sup>Beijing Synchrotron Radiation Facility, Institute of High Energy Physics, Chinese Academy of Sciences Beijing 100084, China.

<sup>d</sup>School of Chemical and Biomedical Engineering, Nanyang Technological University, 62 Nanyang Drive, Singapore 637459, Singapore.

<sup>e</sup>Center for Electron Microscopy, Tianjin University of Technology Tianjin 300384, China.

‡ These authors contributed equally.

*Corresponding authors:* D. Wang (wangdingsheng@mail.tsinghua.edu.cn), Y. Li (ydli@mail.tsinghua.edu.cn)

## 1. Materials and characterizations

**Chemicals:** Analytical grade iron(II) acetate tetrahydrate anhydrous ( $\text{Fe}(\text{oAc})_2$ ), sodium chloride ( $\text{NaCl}$ ), potassium chloride ( $\text{KCl}$ ) and sodium sulfate anhydrous ( $\text{Na}_2\text{SO}_4$ ) was obtained from Sinopharm Chemical, 5, 10, 15, 20-tetra(4-(imidazol-1-yl)phenyl)porphyrindine (TIPP) and  $\alpha,\alpha'$ -Dibromo-p-xylene were purchased from Shanghai Chemical Reagents, China. The commercial Pt/C catalyst purchased from JM Co. is 20% by wt. of  $\sim 3$  nm platinum nanoparticles on XC-72 carbon. Nafion D-521 dispersion (5% w/w in water and 1-propanol) was obtained from Alfa Aesar. The distilled water used in all experiments was obtained through ion-exchange and filtration. All of the chemicals used in this experiment were analytical grade and used without further purification.

**Preparation of  $\text{SiO}_2$  template:** The preparation of different sized silica spheres involves the ammonia-catalyzed hydrolysis and condensation of TEOS in an aqueous ethanol solution via the classical stöber method.<sup>1,2</sup> Taking the synthesis of  $\sim 190$  nm silica spheres as an example, 15 mL of absolute ethanol, 5 mL of DI water, and 0.7 mL of 28%  $\text{NH}_3 \cdot \text{H}_2\text{O}$  were mixed and stirred. A total of 0.6 mL of TEOS was added into the mixture quickly. After a reaction time of about 10 h, the silica spheres were isolated by centrifugation. Then the white precipitate was washed with ethanol three times and dried application.

**Preparation of Fe-TIPP:** In a typical procedure,  $\text{Fe}(\text{oAc})_2$  (104.4 mg, 0.60 mmol) was dissolved in 50ml N, N-dimethylformamide (DMF) to form a clear pink solution, which was subsequently injected into 50ml of DMF containing 175 mg TIPP at room temperature. The mixed solution was then transferred into 250 ml round bottle flask and refluxed at 175 °C for 3 h, evaporated DMF for 80 mL (Scheme S1). The residual solution cooled down room temperature and added in 200 mL freezing-water, then placed 1 h. The as-obtained precipitates was centrifuged and washed with water several times and dried in vacuum at 120 °C for 4 h.

**Preparation of FeCl<sub>11</sub>N<sub>4</sub>/CNS catalyst:** The first, according to the method reported by Wang et al<sup>3</sup>,  $\alpha,\alpha'$ -dibromo-p-xylene (179.5 mg, 0.68 mmol) was dissolved in 20 ml DMF to form a

clear solution, which was subsequently added into 100 mL of DMF containing as-prepared Fe-TIPP (20 mg, 0.02 mmol) and TIPP (280 mg, 0.32 mmol) and SiO<sub>2</sub> (500 mg) under robust stirring at room temperature. The mixed suspension was then transferred into 250 ml round bottle flask at 110 °C for 24 h. The obtained product was separated by centrifugation and washed subsequently with DMF for third and ethanol for twice and finally dried at 80 °C under vacuum for overnight. Then, the collected solid powder (SiO<sub>2</sub>@Fe-TIPP/TIPP-polymer, Fig. S1) and the mixture (placed in upwind) of NaCl (10 mmol), KCl (10 mmol) and Na<sub>2</sub>SO<sub>4</sub> (10 mmol) were placed in a tube furnace and then heated to 800 °C for 3 h at the heating rate of 5 °C /min under flowing H<sub>2</sub>/Ar (5/95 by H<sub>2</sub> and argon) gas and then naturally cooled to room temperature to obtain the representative samples. Then obtained samples were etched in HF aqueous solution at room temperature for 24 h to remove the SiO<sub>2</sub> template and collected by centrifugation, washed subsequently with water and ethanol for third and finally dried at 30 °C under vacuum for overnight.

**Preparation of FeN<sub>4</sub>/CNS catalyst:** The as-fabricated solid powder (SiO<sub>2</sub>@Fe-TIPP/TIPP-polymer) by above method and Na<sub>2</sub>SO<sub>4</sub> (10 mmol) (placed in upwind) were placed in a tube furnace and then heated to 800 °C for 3 h at the heating rate of 5 °C /min under flowing H<sub>2</sub>/Ar (5/95 by H<sub>2</sub> and argon) gas and then naturally cooled to room temperature to obtain the representative samples. Then obtained samples were etched in HF aqueous solution at room temperature for 24 h to remove the SiO<sub>2</sub> template and collected by centrifugation, washed subsequently with water and ethanol for third and finally dried at 30 °C under vacuum for overnight.

**Preparation of FeN<sub>4</sub>/CN catalyst:** The as-fabricated solid powder (SiO<sub>2</sub>@Fe-TIPP/TIPP-polymer) by above method was placed in a tube furnace and then heated to 800 °C for 3 h at the heating rate of 5 °C /min under flowing H<sub>2</sub>/Ar (5/95 by H<sub>2</sub> and argon) gas and then naturally cooled to room temperature to obtain the representative samples. Then obtained samples were etched in HF aqueous solution at room temperature for 24 h to remove the SiO<sub>2</sub> template and

collected by centrifugation, washed subsequently with water and ethanol for third and finally dried at 30 °C under vacuum for overnight.

**Characterization:** Powder X-ray diffraction patterns of samples were recorded using a Rigaku RU-200b X-ray powder diffractometer (XRD) with Cu K $\alpha$  radiation ( $\lambda = 1.5406 \text{ \AA}$ ). TEM images were performed on a Hitachi H-800 transmission electron microscope. The high-resolution TEM, HAADF-STEM images and elemental mapping were recorded on a JEOL-2100F FETEM with electron acceleration energy of 200 kV. The scanning electron microscope (SEM) was carried out by a JSM-6700F SEM. Photoemission spectroscopy experiments (XPS) were performed at the Catalysis and Surface Science End station at the BL11U beamline of National Synchrotron Radiation Laboratory (NSRL) in Hefei, China. Elemental analysis of Fe in the solid samples was detected by an Optima 7300 DV inductively coupled plasma atomic emission spectrometer (ICP-AES).

**XAFS measurement:** The X-ray absorption fine structure spectra (Fe K-edge) were collected at 1W1B station in Beijing Synchrotron Radiation Facility (BSRF). The storage rings of BSRF was operated at 2.5 GeV with a maximum current of 250 mA. Using Si(111) double-crystal monochromator, the data collection was carried out in transmission mode using ionization chamber for Fe foil, Fe<sub>2</sub>O<sub>3</sub>, and in fluorescence excitation mode using a Lytle detector for FeCl<sub>11</sub>N<sub>4</sub>/CNS, FeN<sub>4</sub>/CNS and FeN<sub>4</sub>/CN. All spectra were collected in ambient conditions.

**XAFS Analysis and Results:** The acquired EXAFS data were processed according to the standard procedures using the ATHENA module implemented in the IFEFFIT software packages. The  $k^3$ -weighted EXAFS spectra were obtained by subtracting the post-edge background from the overall absorption and then normalizing with respect to the edge-jump step. Subsequently,  $k^3$ -weighted  $\chi(k)$  data of Fe K-edge were Fourier transformed to real (R) space using a hanning windows ( $dk=1.0 \text{ \AA}^{-1}$ ) to separate the EXAFS contributions from different coordination shells. To obtain the quantitative structural parameters around central

atoms, least-squares curve parameter fitting was performed using the ARTEMIS module of IFEFFIT software packages. The following EXAFS equation was used:

$$\chi(k) = \sum_j \frac{N_j S_0^2 F_j(k)}{k R_j^2} \exp[-2k^2 \sigma_j^2] \exp\left[-\frac{2R_j}{\lambda(k)}\right] \sin[2k R_j + \phi_j(k)]$$

$S_0^2$  is the amplitude reduction factor,  $\phi_j(k)$  is the effective curved-wave backscattering amplitude,  $N_j$  is the number of neighbors in the  $j^{\text{th}}$  atomic shell,  $R_j$  is the distance between the X-ray absorbing central atom and the atoms in the  $j^{\text{th}}$  atomic shell (backscatterer),  $\lambda$  is the mean free path in Å,  $\phi_j(k)$  is the phase shift (including the phase shift for each shell and the total central atom phase shift),  $\sigma_j$  is the Debye-Waller parameter of the  $j^{\text{th}}$  atomic shell (variation of distances around the average  $R_j$ ). The functions  $F_j(k)$ ,  $\lambda$  and  $\phi_j(k)$  were calculated with the ab initio code FEFF 8.2.

**Electrochemical measurements:** All catalysts were prepared by mixing 5 mg of the catalyst in 1 ml of solution containing 470  $\mu\text{L}$  of ethanol, 470  $\mu\text{L}$  of  $\text{H}_2\text{O}$  and 60  $\mu\text{L}$  of 5% Nafion solution, followed by ultrasonication for 30 min to form homogeneous catalyst inks. While, commercial 20 % wt Pt/C sample was prepared by dispersing 4 mg of the catalyst in 1 ml of solution. Next, a certain volume of the catalyst ink was carefully dropped onto the polished glassy carbon rotating disk electrode (RDE) or rotating ring disk electrode (RRDE), leading to a desirable catalyst loading. In 0.1 M KOH, the nonprecious catalyst loading was 0.501 mg  $\text{cm}^{-2}$  and the loading of Pt/C was 0.102 mg  $\text{cm}^{-2}$ .

Electrochemical measurements were carried out in a three-electrode system on a CHI 760E electrochemical workstation (Shanghai Chenhua, China) in 0.1 M KOH electrolyte. A glassy carbon (GC) RDE of 5 mm in diameter coated with the catalyst ink was served as the working electrode, the Ag/AgCl (saturated KCl solution) and Pt wire were used as reference and counter electrode, respectively. Prior to measurement, a  $\text{N}_2/\text{O}_2$  flow was used through the electrolyte in

the cell for 30 min to saturate it with N<sub>2</sub>/O<sub>2</sub>. The electrochemical experiments were conducted in O<sub>2</sub>-saturated 0.1 M KOH for the oxygen reduction reaction at room temperature, respectively. The RDE tests were measured at various rotating speed from 900 to 2500 rpm with a sweep rate of 10 mV·s<sup>-1</sup>. The cyclic voltammetry (CV) experiments were cycled in N<sub>2</sub>/O<sub>2</sub>-saturated 0.1 M KOH electrolyte solutions with a scan rate of 50 mV·s<sup>-1</sup>, respectively. For the ORR at a RDE, the electron transfer number (n) and kinetic current density (J<sub>k</sub>) were calculated from the Koutecky-Levich equation:

$$\frac{1}{J} = \frac{1}{J_L} + \frac{1}{J_K} = \frac{1}{B\omega^{\frac{2}{3}}} + \frac{1}{J_K}$$

$$B = 0.62nFC_0 D_0^{\frac{2}{3}} V^{-\frac{1}{6}}$$

where  $J$  is the measured current density,  $J_K$  and  $J_L$  are the kinetic and limiting current densities,  $\omega$  is the angular velocity of the disk,  $n$  is the electron transfer number,  $F$  is the Faraday constant (96485 C·mol<sup>-1</sup>),  $C_0$  is the bulk concentration of O<sub>2</sub> (1.2 × 10<sup>-6</sup> mol·cm<sup>-3</sup>),  $D_0$  is the diffusion coefficient of O<sub>2</sub> (1.9 × 10<sup>-5</sup> cm<sup>2</sup>·s<sup>-1</sup>), and  $V$  is the kinematic viscosity of the electrolyte (0.01 cm<sup>2</sup>·s<sup>-1</sup>).

For RRDE tests, a computer-controlled CHI 760E electrochemical workstation was employed and the disk electrode was scanned cathodically at a rate of 10 mV·s<sup>-1</sup> and the ring electrode potential was set to 1.23 V vs. RHE. The hydrogen peroxide yield (H<sub>2</sub>O<sub>2</sub> %) and the electron transfer number (n) were determined by the following equations:

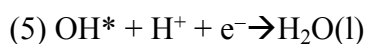
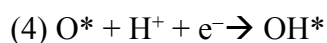
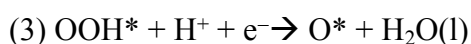
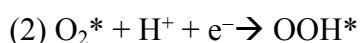
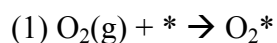
$$\text{H}_2\text{O}_2 (\%) = 200 \times \frac{\frac{I_r}{N}}{I_d + \frac{I_r}{N}}$$

$$n = 4 \times \frac{I_d}{I_d + \frac{I_r}{N}}$$

Where  $I_d$  is the disk current,  $I_r$  is the ring current, and  $N = 0.38$  is the current collection efficiency of the Pt ring.

The accelerated durability tests of the catalysts were performed at room temperature by applying potential cycling between 0.2 and 1.1 V vs. RHE in the O<sub>2</sub>-saturated in the O<sub>2</sub>-saturated 0.1 M KOH electrolyte at a sweep rate of 50 mV·s<sup>-1</sup> for 10000 cycles, respectively.

**Calculation detail:** Since the acid/base condition leads to a constant offset on the free energy difference at a given pH in our model, the simulated condition for ORR is chosen to be the standard condition (pH=1, T=298K and P= 1 bar). All density functional theory calculations were carried out by Dmol<sup>3</sup> program. The generalized-gradient approximation (GGA) with spin polarized Perdew-Burke-Ernzerhof (PBE) functional were employed to describe the exchange-correlation potential<sup>4</sup> and the double numerical plus polarization (DNP) basis set was chosen to describe the valence orbitals of the atoms with the core electrons treated by the effective core potentials (ECP) method.<sup>4b, 4c</sup> To module the FeN<sub>4</sub>/CN electrocatalyst, a Fe-N<sub>4</sub> site was embedded in a periodic 4×4 graphene support (32 carbon sites) with lattice parameters a=b=9.84 Å and γ=120°. The vacuum spacing was set to more than 15Å along the surface normal to avoid the interactions between images. The k-space integration was sampled using a 2×2×1 Monkhorst-Pack grid. In present study, we employed the methodology developed by Norskov et al to explore the electrocatalytic reactivity of singly dispersed Fe catalyst.<sup>4d</sup> The four electron pathway by which the ORR occurs under acid condition are generally reported to proceed according to the following steps:

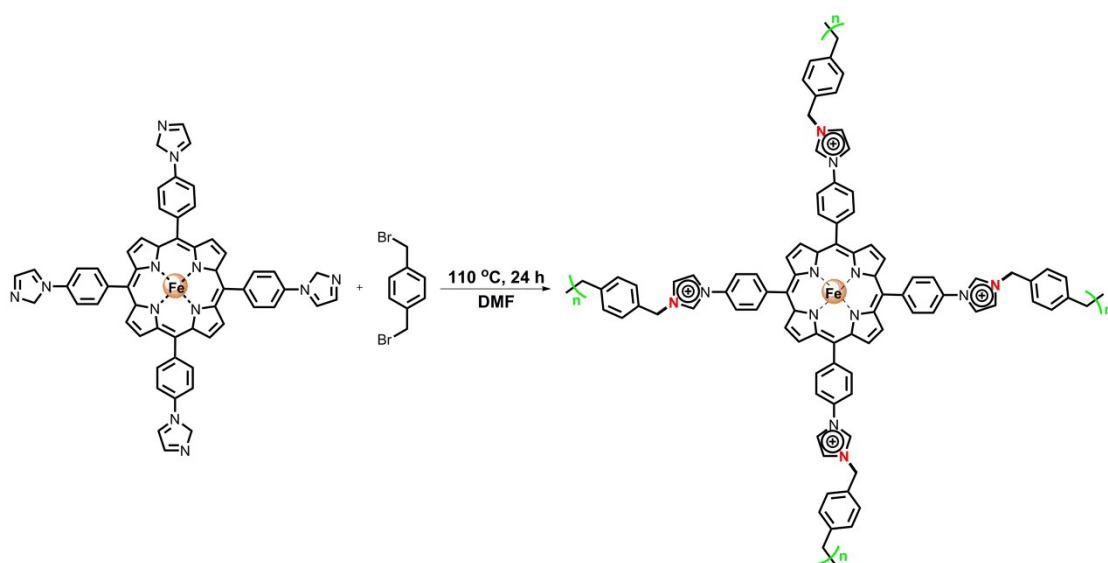


The chemical potential for the reaction ( $\text{H}^+ + \text{e}^-$ ) (i.e. the free energy per H) is equal to that of  $1/2\text{H}_2$  by setting the reference potential to be that of the standard hydrogen electrode at standard condition ( $\text{pH}=0$ ,  $P_{\text{H}_2}=1\text{bar}$ , and  $T=298\text{ K}$ ). The reaction free energy ( $\Delta G$ ) is further calculated by the formula:

$$\Delta G = \Delta H - T\Delta S - qU + k_B T \ln 10 * (\text{pH}),$$

Where  $\Delta H$  is the reaction enthalpy of an elementary step in ORR and is estimated by the reaction energy ( $\Delta E$ ) from DFT calculations with zero-point energy (ZPE) correction;  $T\Delta S$  is the change in entropy contribution to the free energy;  $U$  is the applied potential;  $q$  is the charge transfer in each elementary step. Note that the entropic and zero point energies contributions are considered not distinctly different for all the system and are obtained based on the results for Fe-N4 system. The entropy for liquid water is taken from Ref. 4d but we note that the solvation effect was not consider for the system. Since DFT cannot accurately describe the ground state of  $\text{O}_2$ , the free energy of  $\text{O}_2$  is manually estimated by setting the equilibrium potential ( $U_0$ ) for water dissociation to be 1.23V under standard condition. The overpotential  $\phi$  is defined as the potential above which all the four free-energy pathways become downhill and the values reported in the current manuscript are all respected to the equilibrium potential  $U_0$  (i.e.  $\phi = U_0 - U$ ) in Fig. S30-S33. See the work by Noskov et al for details.<sup>4d</sup>

## 2. Supplementary Figures and Tables



**Scheme S1** The reaction of Quaterisation.

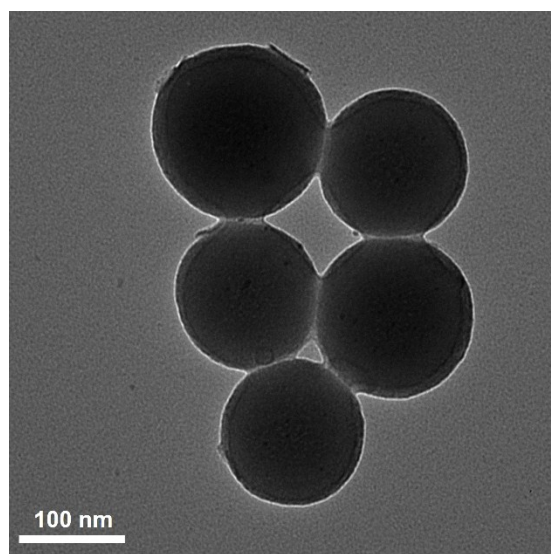


**Fig. S1** TEM images of SiO<sub>2</sub>@Fe-TIPP/TIPP-polymer.

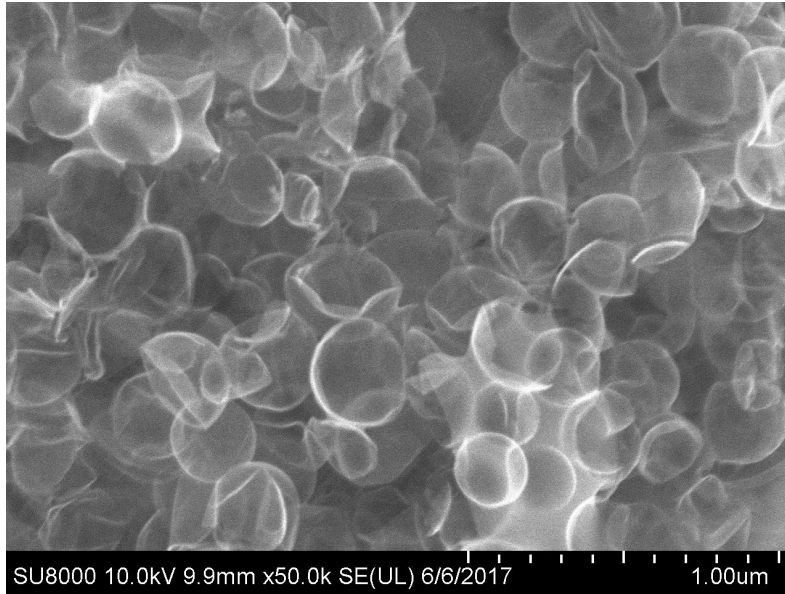


Fig. S2 SEM image of FeCl1N4/CNS.

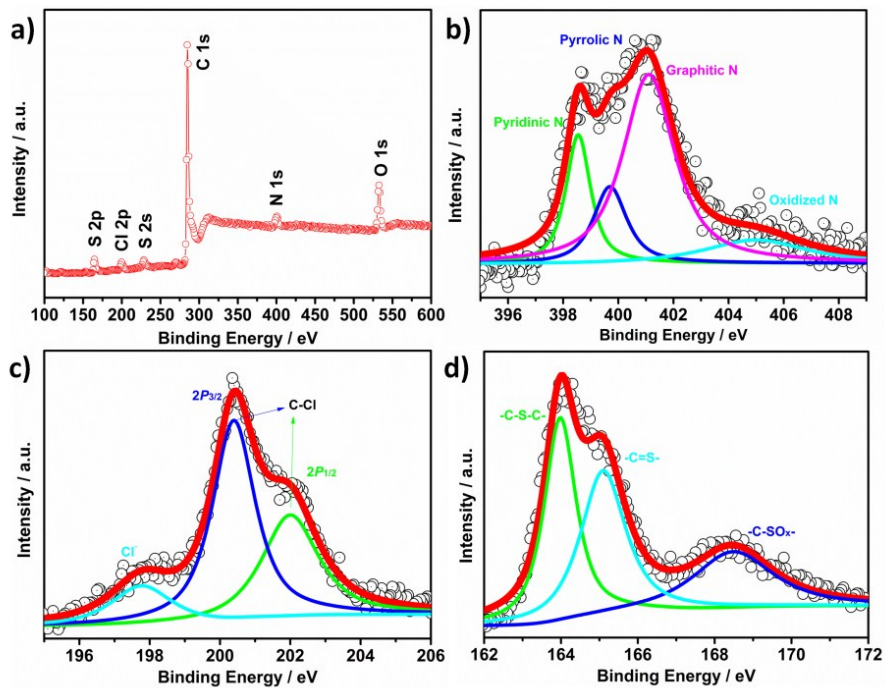


Fig. S3 XPS survey spectra for (a) survey spectrum; (b) the N 1s regions; (c) the Cl 2p regions and the S 2p regions of FeCl1N4/CNS.

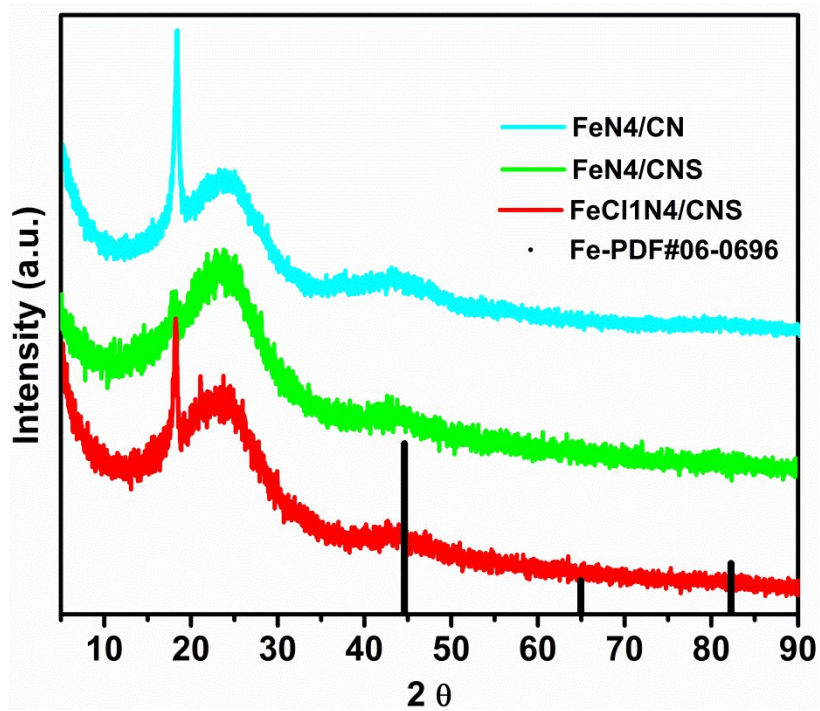


Fig. S4 XRD patterns of FeCl1N4/CNS, FeN4/CNS and FeN4/CN.

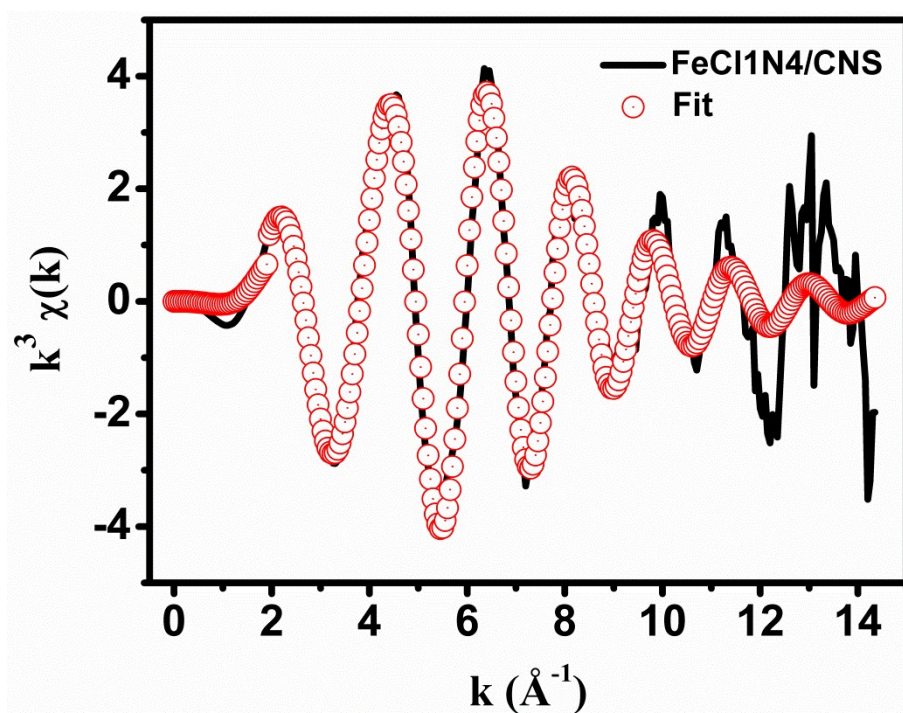


Fig. S5 Corresponding EXAFS fitting curves of FeCl1N4/CNS at k space.

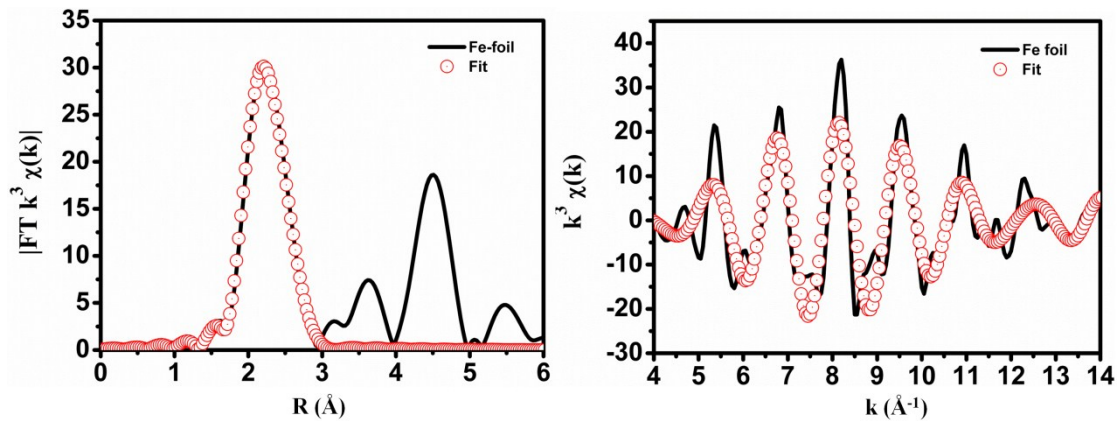


Fig. S6 The corresponding EXAFS fitting curves of Fe foil.

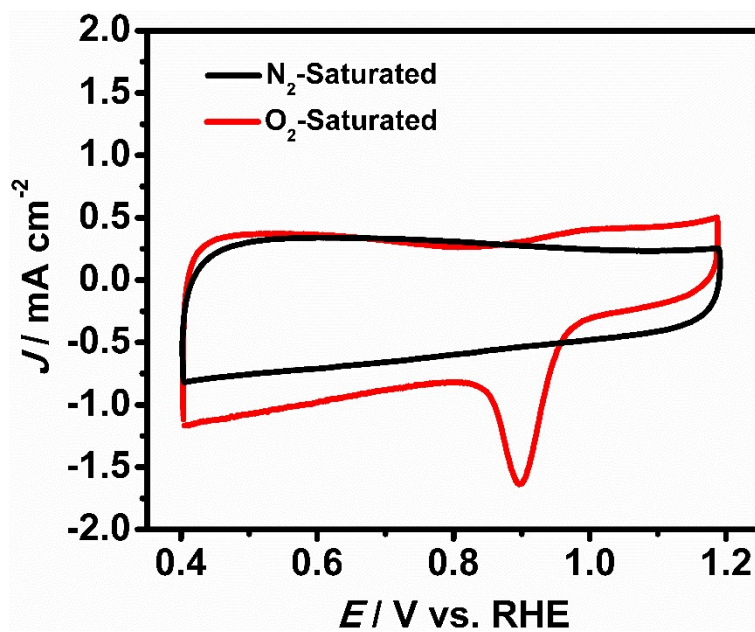
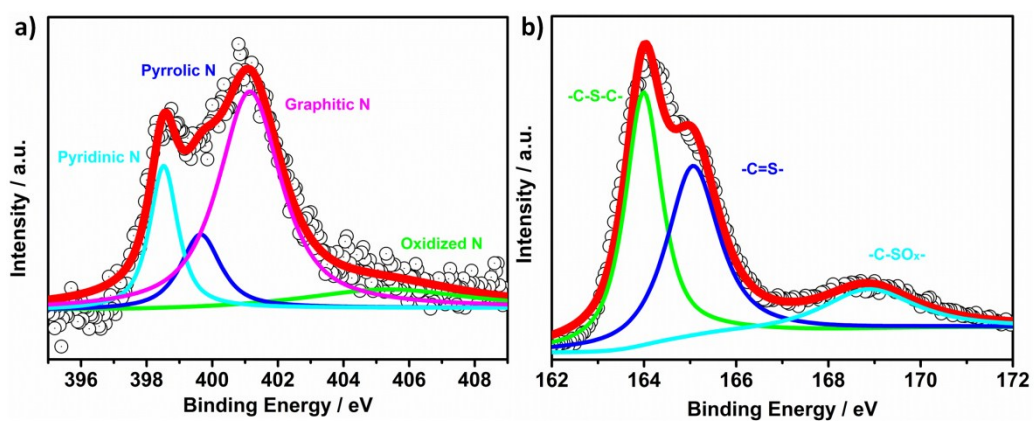
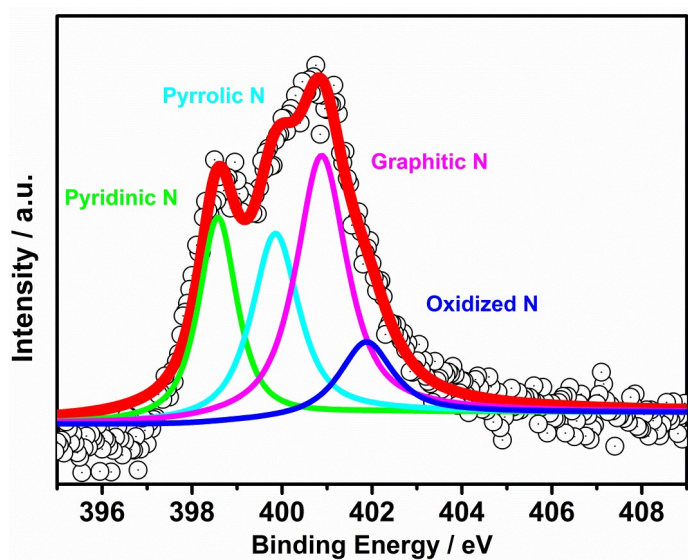


Fig. S7 CVs of FeCl<sub>11</sub>N<sub>4</sub>/CNS catalyst in O<sub>2</sub>-saturated and N<sub>2</sub>-saturated 0.1 M KOH.



**Fig. S8** XPS survey spectra for (a) the N 1s regions and the S 2p regions of FeN<sub>4</sub>/CNS.



**Fig. S9** XPS spectra for the N 1s regions of FeN<sub>4</sub>/CN.

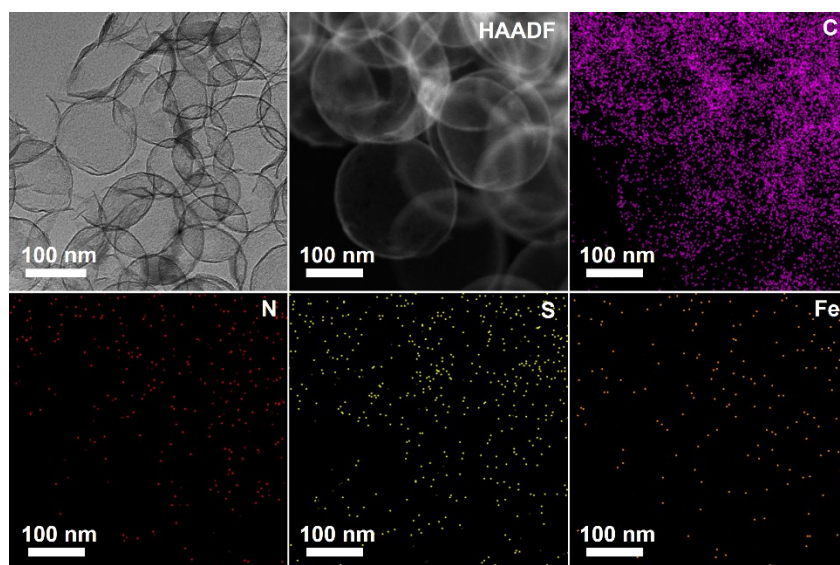


**Fig. S10** TEM images, HAADF-STEM image and corresponding EDX element mapping of FeN<sub>4</sub>/CNS, C (violet), N (red), S (yellow) and Fe (orange).

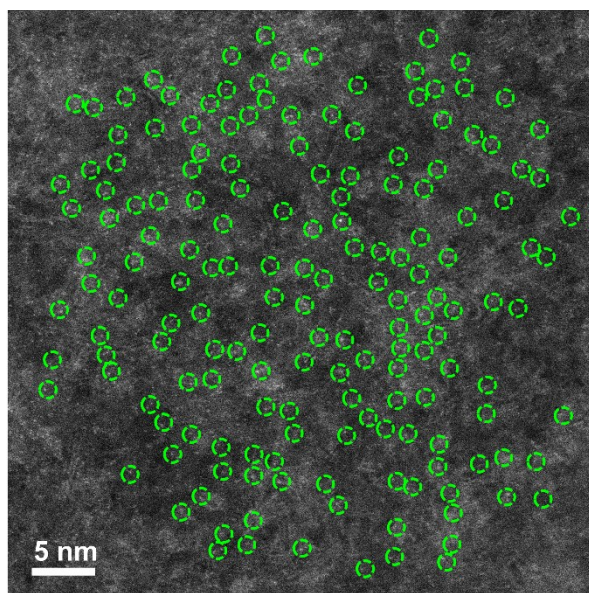


**Fig. S11** AC HAADF-STEM image of FeN<sub>4</sub>/CNS.

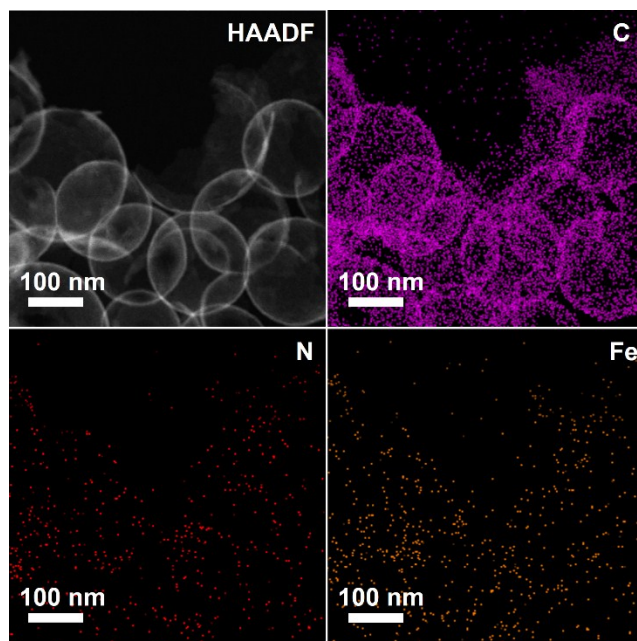


**Fig. S12** HAADF-STEM image and corresponding EDX element mapping of FeN<sub>4</sub>/CN, C (violet), N (red) and Fe (orange).

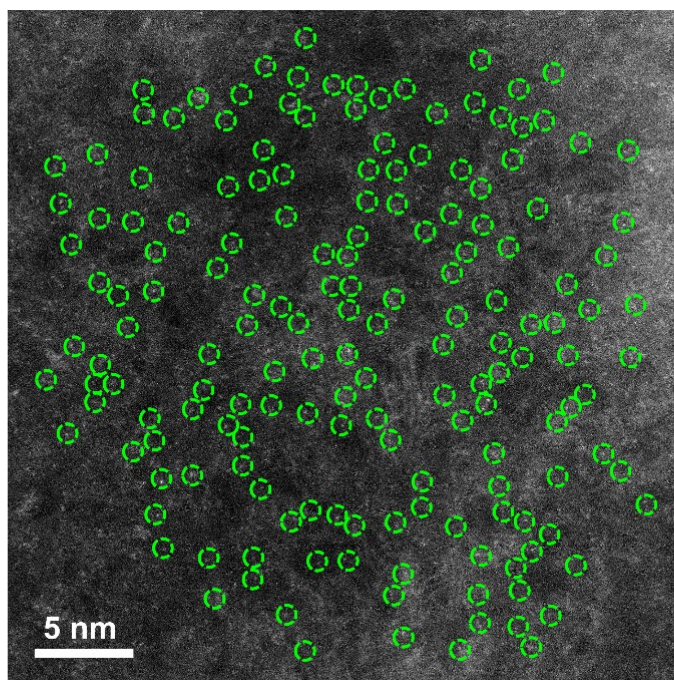


**Fig. S13** AC HAADF-STEM image of FeN<sub>4</sub>/CN.

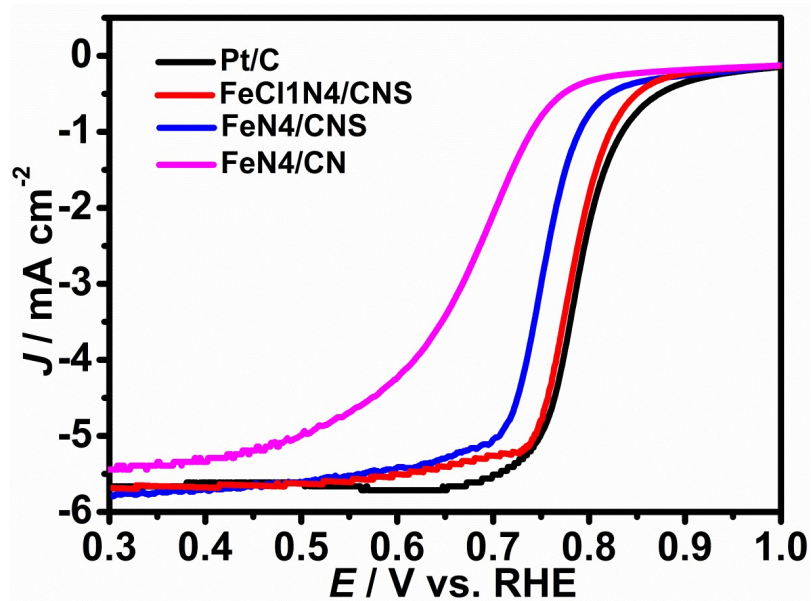


Fig. S14 ORR polarization curves in  $O_2$ -saturated 0.5 M  $H_2SO_4$ .

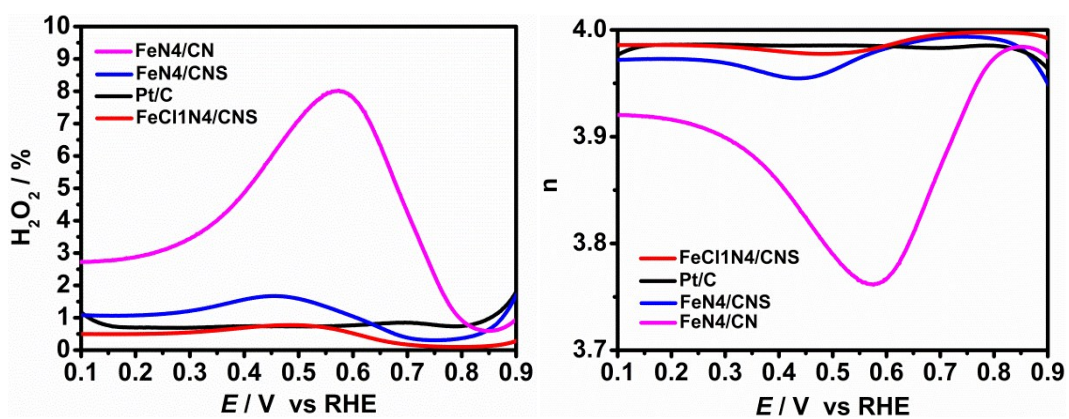
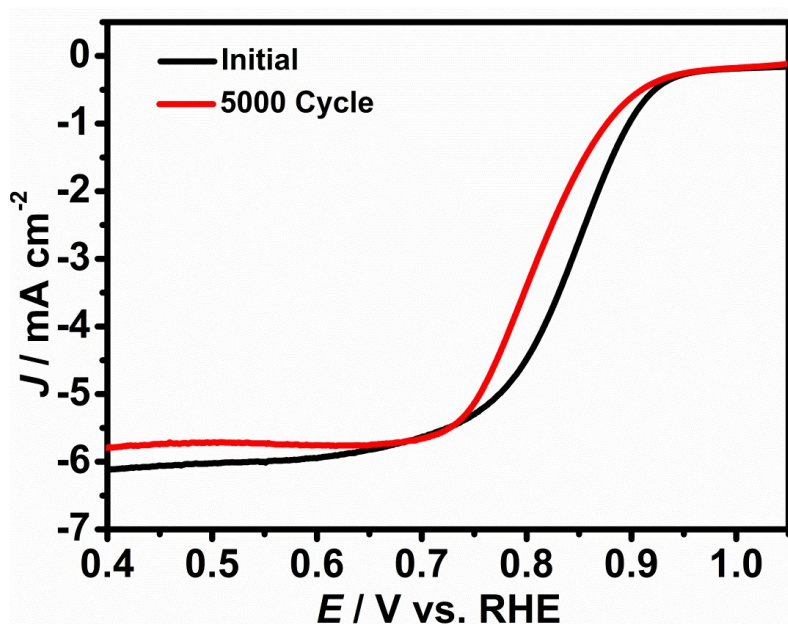
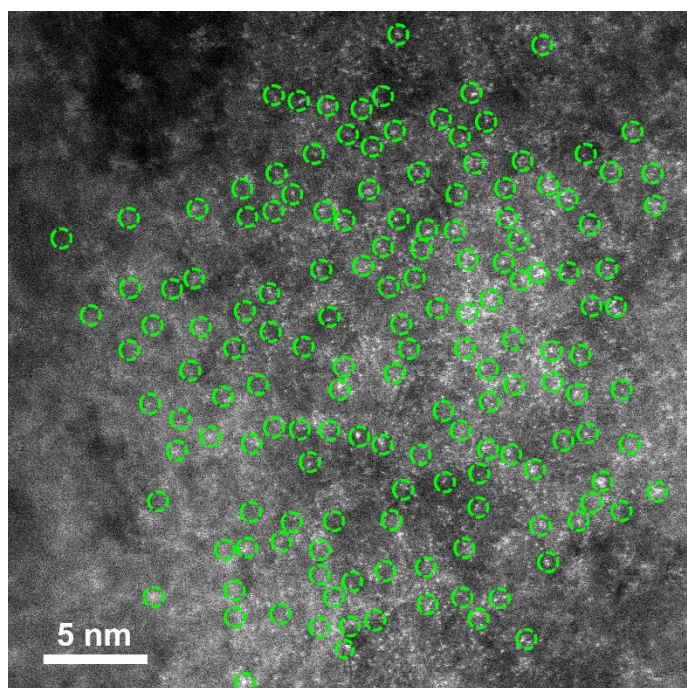


Fig. S15  $H_2O_2$  yield plots and electron transfer numbers plots in 0.1 M  $KOH$ .



**Fig. S16** ORR polarization curves before and after 5000 potential cycles for Pt/C in 0.1 M KOH.



**Fig. S17** AC HAADF-STEM image of FeCl<sub>1</sub>N<sub>4</sub>/CNS after CVs of 5000 cycles at a scan rate of 50 mV/s in 0.1 M KOH.

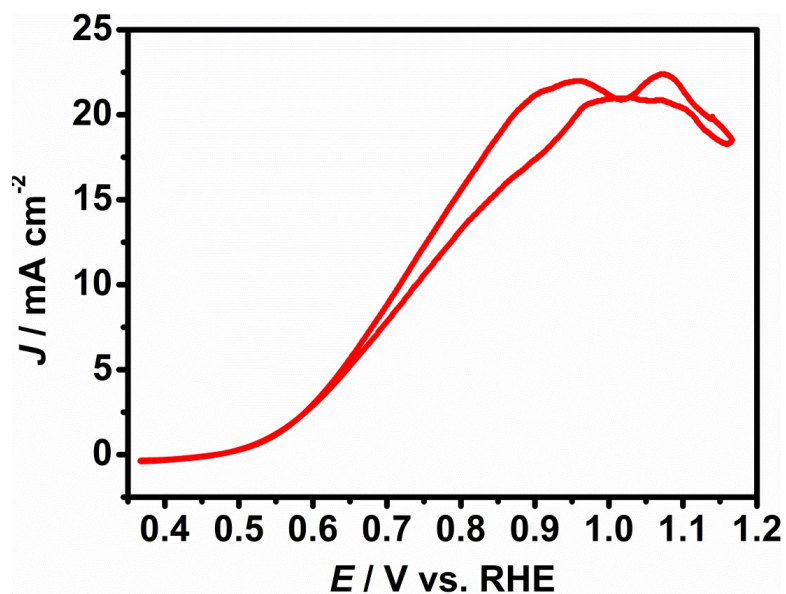


**Fig. S18** CVs of Pt/C in O<sub>2</sub>-saturated 0.1 M KOH without and with 1.0 M CH<sub>3</sub>OH at a scan rate of 10 mV/s.

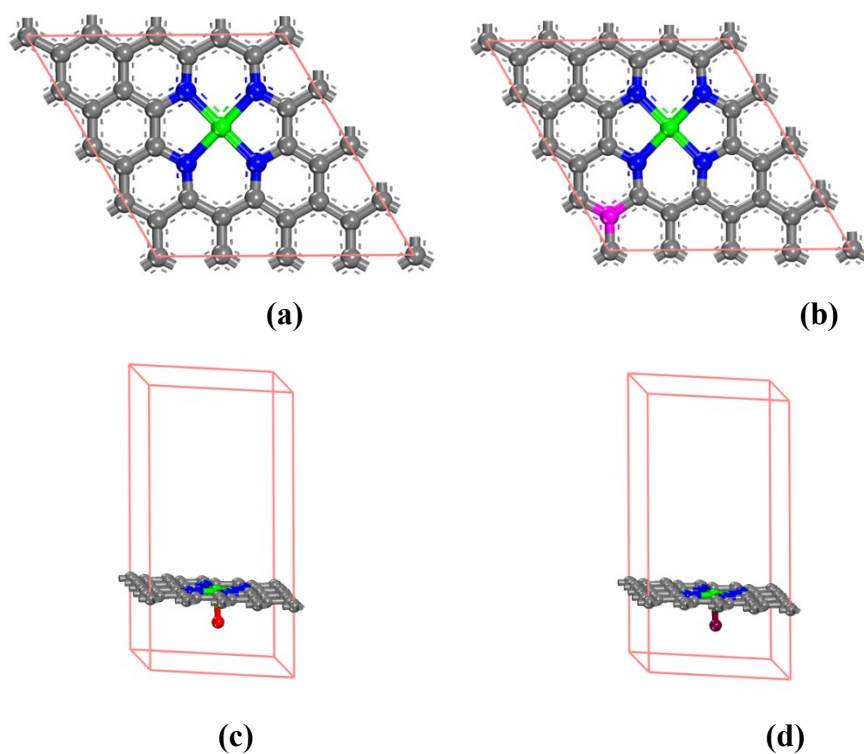


**Fig. S19** Structural models: (a) FeN<sub>4</sub>/CN catalyst, (b) FeN<sub>4</sub>/CNS, (c) FeO<sub>1</sub>N<sub>4</sub>/CN, and (d) FeCl<sub>1</sub>N<sub>4</sub>/CNS. We did not consider Cl doped into the substrate because its covalent coordination number is 1 at maximum.

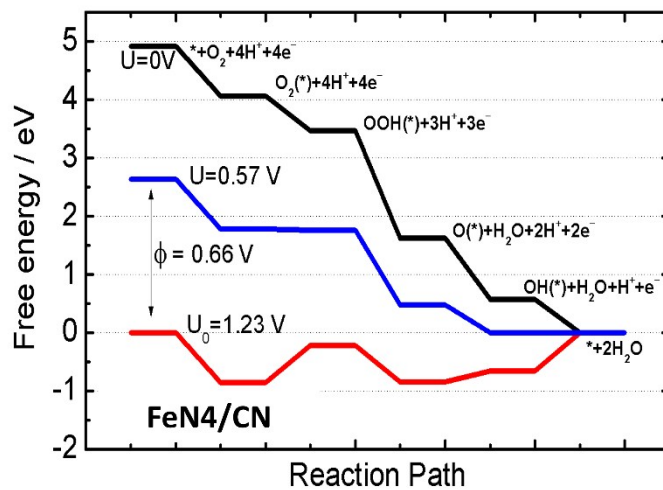


**Fig. S20** Free energy paths of ORR on FeN4/CN model at pH=0 and T=298 K.

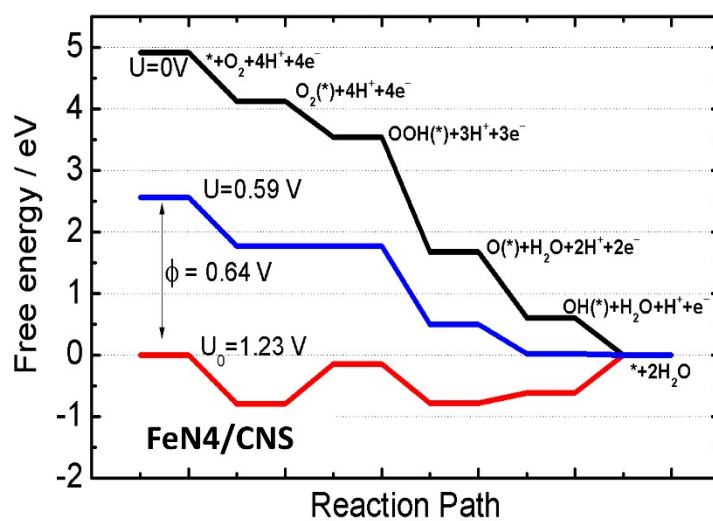


**Fig. S21** Free energy paths of ORR on FeN4/CNS model at pH=0 and T=298 K.

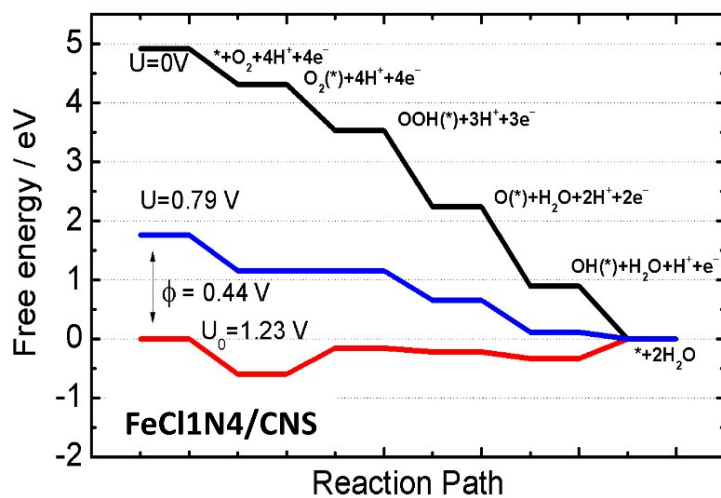


**Fig. S22** Free energy paths of ORR on FeCl1N4/CNS model at pH=0 and T=298 K.

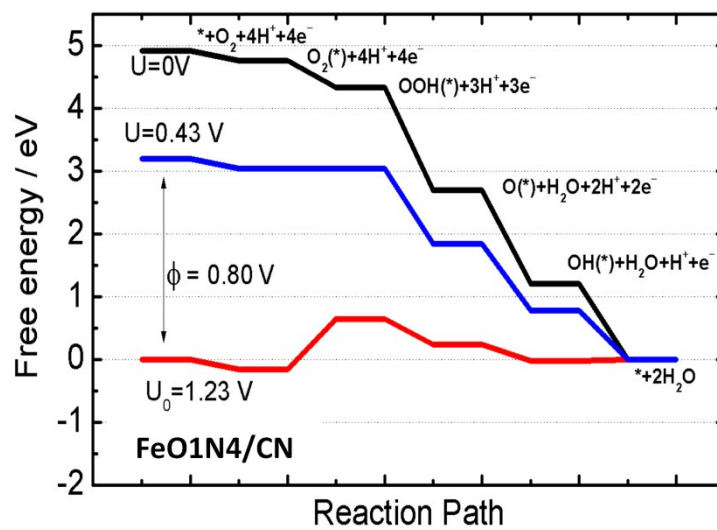


**Fig. S23** Free energy paths of ORR on FeO1N4/CN model at pH=0 and T=298 K.

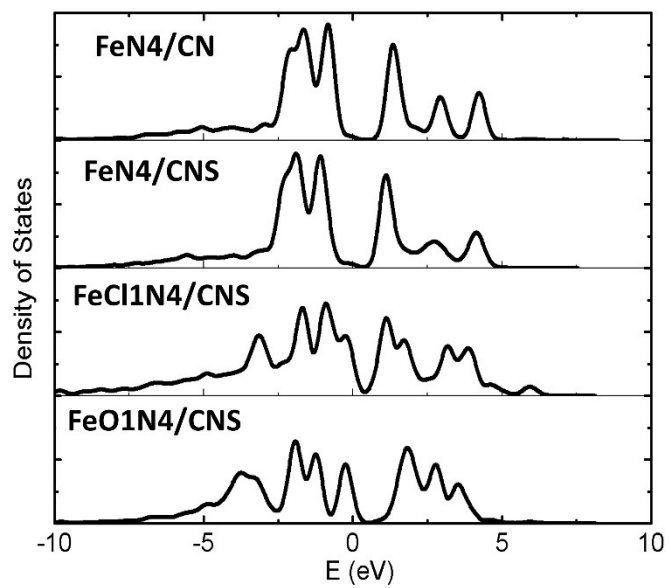


**Fig. S24** Partial density of states (DOS) for Fe *d* band in different types of electrocatalysts

**Table S1.** Structural parameters of FeCl1N4/CNS extracted from the EXAFS fitting.

$$(S_0^2=0.85).$$

Sample	Scattering Pair	CN	R (Å)	$\sigma^2$ ( $10^{-3}$ Å <sup>2</sup> )	$\Delta E_0$ (eV)	R factor
FeCl1N4/CNS	Fe-N	1.4	1.92	6.5	2.5	0.0048
	Fe-NCl	3.6	2.19	7.2	3.1	
Fe foil	Fe-Fe <sub>1</sub>	8	2.46	4.4	4.6	0.0063
	Fe-Fe <sub>2</sub>	6	2.84	4.5	4.1	

$S_0^2$  is the amplitude reduction factor; CN is the coordination number; R is interatomic distance (the bond length between central atoms and surrounding coordination atoms);  $\sigma^2$  is Debye-Waller factor (a measure of thermal and static disorder in absorber-scatterer distances);  $\Delta E_0$  is edge-energy shift (the difference between the zero kinetic energy value of the sample and that of the theoretical model). R factor is used to value the goodness of the fitting.

\* This value was fixed during EXAFS fitting, based on the known structure.

Error bounds that characterize the structural parameters obtained by EXAFS spectroscopy were estimated as  $N \pm 20\%$ ;  $R \pm 1\%$ ;  $\sigma^2 \pm 20\%$ ;  $\Delta E_0 \pm 20\%$ .

FeCl1N4/CNS (FT range: 2.0-11.8 Å<sup>-1</sup>; fitting range: 0.5-2.5 Å)

**Table S2.** Mössbauer Parameters of FeCl1N4/CNS.  $\delta_{iso}$  = Chemical Shift,  $\Delta E_Q$  = Quadrupole splitting.

Doublet	$\delta_{iso}/\text{mm s}^{-1}$	$\Delta E_Q/\text{mm s}^{-1}$	Area (%)
<b>D1</b>	0.36	0.97	31.7
<b>D2</b>	0.47	1.81	23.6
<b>D3</b>	0.21	2.98	33.4
<b>D4</b>	0.91	3.56	11.3

**Table S3.** Comparison of ORR activity of various non-precious catalysts in 0.1 M KOH.

Catalysts	Half-wave	Rotation and scan rate	Decay	Ref.
<b>FeCl1N4/CNS</b>	<b>0.921 V (vs. RHE)</b>	<b>1600 rpm and 10 mV s<sup>-1</sup></b>	<b>3 mV</b>	<b>This work</b>
FeN4/CNS	0.884 V (vs. RHE)	1600 rpm and 10 mV s <sup>-1</sup>	--	This work
FeN4/CN	0.835 V (vs. RHE)	1600 rpm and 10 mV s <sup>-1</sup>	--	This work
Fe-ISAs/CN	0.900 (V vs RHE)	1600 rpm and 10 mV s <sup>-1</sup>	2 mV	5
Fe-N <sub>x</sub> /C (0.1 M NaOH)	0.837 (V vs RHE)	900 rpm and 20 mV s <sup>-1</sup>	--	6
Fe <sub>3</sub> C/C-800	0.86 (V vs RHE)	900 rpm and 10 mV s <sup>-1</sup>	20 mV	7
(Fe,Mn)-N-C	0.900 (V vs RHE)	1500 rpm and 10 mV s <sup>-1</sup>	1% (4500 Cycles)	8
BCNFNHs	0.861 (V vs RHE)	1600 rpm and 5 mV s <sup>-1</sup>	1 mV (3000 Cycles)	9

		1		
Fe-N/C-800	0.81 (V vs RHE)	1600 rpm and 10 mV s <sup>-1</sup>	6.7% (10000 s)	10
FePhen@MOF-ArNH <sub>3</sub>	0.86 (V vs RHE)	1600 rpm and 20 mV s <sup>-1</sup>	--	11
Fe@C-FeNCs-2	0.899 (V vs RHE)	1600 rpm and 10 mV s <sup>-1</sup>	16 mV	12
CNT/PC	0.88 (V vs RHE)	1600 rpm and 10 mV s <sup>-1</sup>	1 mV (10000 Cycles)	13
NT-G	0.87 (V vs RHE)	1600 rpm and 5 mV s <sup>-1</sup>	--	14
N-doped C/CNTs	0.82 (V vs RHE)	1600 rpm and 5 mV s <sup>-1</sup>	4.5% (10000 Cycles)	15
Meso/micro-PoPD	0.85 (V vs RHE)	1600 rpm and 10 mV s <sup>-1</sup>	10 mV (10000 Cycles)	16
NCNTFs	0.87 (V vs RHE)	1600 rpm and 10 mV s <sup>-1</sup>	7 mV (5000 Cycles)	17

Co SAs/N-C(900)	0.881 (V vs RHE)	1600 rpm and 10 mV s <sup>-1</sup>	3 mV (5000 Cycles)	18
-----------------	------------------	------------------------------------	--------------------	----

**Table S4.** Energetic and electronic parameters for different types of electro-catalysts.

Models	Overpotential $\phi$ (V)	Charge of Fe $q$ ( $e$ )	O <sub>2</sub> binding energy $E_b$ (eV)
FeN4	0.66	0.61	-0.80
FeN4/CNS	0.64	0.61	-0.79
FeCl1N4/CNS	0.44	0.63	-0.64
FeO1N4/CN	0.80	0.72	-0.23
Fe <sub>6</sub> cluster	1.77	0.00	-1.52

### 3. References

- [1] W. Stöber, A. Fink, E. Bohn, *J. Colloid Interface Sci.*, 1968, **26**, 62.
- [2] R. Mayoral, J. Requena, J. S. Moya, C. Lopez, A. Cintas, H. Miguez, F. Meseguer, L. Vazquez, M. Holgado, A. Blanco, *Adv. Mater.*, 1997, **9**, 257.
- [3] Y. X. Wang, H. X. Zhao, X. X. Li and R. H. Wang, *J. Mater. Chem. A*, 2016, **4**, 12554.
- [4] (a) J. P. Perdew, K. Burke, and M. Ernzerhof, *Phys. Rev. Lett.*, 1996, **77**, 3865. (b) B. Delley, *J. Chem. Phys.*, 1990, **92**, 508. (c) B. Delley, *J. Chem. Phys.*, 2000, **113**, 7756. (d) J. K. Nørskov, J. Rossmeisl, A. Logadottir, and L. Lindqvist, *J. Phys. Chem. B*, 2004, **108**, 17886.
- [5] Y. J. Chen, S. F. Ji, Y. G. Wang, J. C. Dong, W. X. Chen, Z. Li, R. A. Shen, L. R. Zheng, Z. B. Zhuang, D. S. Wang, Y. D. Li, *Angew. Chem. Int. Ed.*, 2017, **56**, 6937.
- [6] N. Ramaswamy, U. Tylus, Q. Y. Jia, and S. Mukerjee, *J. Am. Chem. Soc.*, 2013, **135**, 15443.
- [7] Y. Hu, J. O. Jensen, W. Zhang, L. N. Cleemann, W. Xing, N. J. Bjerrum, and Q. F. Li, *Angew. Chem. Int. Ed.*, 2014, **53**, 3675.
- [8] N. R. Sahraie, U. I. Kramm, J. Steinberg, Y. J. Zhang, A. Thomas, T. Reier, J.-P. Paraknowitsch, and P. Strasser, *Nat. Commun.*, 2015, **6**, 8618.
- [9] W. X. Yang, X. J. Liu, X. Y. Yue, J. B. Jia, and S. Guo, *J. J. Am. Chem. Soc.*, 2015, **137**, 1436.
- [10] W. H. Niu, L. G. Li, X. J. Liu, N. Wang, J. Liu, W. J. Zhou, Z. H. Tang, and S. W. Chen, *J. Am. Chem. Soc.*, 2015, **137**, 5555.

- [11]W. J. Jiang, L. Gu, L. Li, Y. Zhang, X. Zhang, L. J. Zhang, J. Q. Wang, J. S. Hu, Z. D. Wei, and L. J. Wan, *J. Am. Chem. Soc.*, 2016, **138**, 3570.
- [12]K. Strickland, E. Miner, Q. Y. Jia, U. Tylus, N. Ramaswamy, W. T. Liang, M.-T. Sougrati, F. Jaouen, and S. Mukerjee, *Nat. Commun.*, 2015, **6**, 7343.
- [13]Y. Sa, D. Seo, J. Woo, J. Lim, J. Cheon, S. Yang, J. Lee, D. Kang, T. Shin, H. Shin, H. Jeong, C. Kim, M. Kim, T. Kim, S. Joo, *J. Am. Chem. Soc.*, 2016, **138**, 15046.
- [14]Y. G. Li, W. Zhou, H. L. Wang, L. M. Xie, Y. Y. Liang, F. Wei, J. C. Idrobo, S. J. Pennycook, and H. J. Dai, *Nat. Nanotechnol.*, 2012, **7**, 394.
- [15]Y. J. Sa, C. Park, H. Y. Jeong, S.-H. Park, Z. Lee, K. T. Kim, G.-G. Park, and S. H. Joo, *Angew. Chem. Int. Ed.*, 2014, **53**, 4102.
- [16]H. W. Liang, X. D. Zhuang, S. Brüller, X. L. Feng, and K. Müllen, *Nat. Commun.*, 2014, **5**, 4973.
- [17]B. Y. Xia, Y. Yan, N. Li, H. B. Wu, X. W. (David) Lou, and X. Wang, *Nat. Energy*, 2016, **1**, 15006.
- [18]P. Q. Yin, T. Yao, Y. E. Wu, L. R. Zheng, Y. Lin, W. Liu, H. X. Ju, J. F. Zhu, X. Hong, Z. X. Deng, G. Zhou, S. Q. Wei, Y. D. Li, *Angew. Chem. Int. Ed.*, 2016, **55**, 10800.